Hemisphere, Washington, DC, 1981.
[3]Howell, J. R., *A Catalog of Radiation Configuration Factors*, McGraw-Hill, New York, 1982.
[4]Gross, U., Spindler, K., and Hahne, E., "Shapefactor-Equations for Radiation Heat Transfer Between Plane Rectangular Surfaces of Arbitrary Position and Size with Parallel Boundaries," *Letters in Heat and Mass Transfer*, Vol. 8, No. 3, 1981, pp. 219–227.
[5]Sanchez, A., and Smith, T. F., "Surface Radiation Exchange for Two-Dimensional Rectangular Enclosures Using the Discrete-Ordinates Method," *Journal of Heat Transfer*, Vol. 114, May 1992, pp. 465–472.
[6]Wolfram, S., *Mathematica®: A System for Doing Mathematics by Computer*, Addison-Wesley, New York, 1988.
[7]Chapman, A. J., *Fundamentals of Heat Transfer*, Macmillan, New York, 1987, p. 549.

Adaptive Grid Generation for the Calculation of Radiative Configuration Factors

C. J. Saltiel* and J. Kolibal†
University of Florida, Gainesville, Florida 32611

Introduction

MANY practical thermal and optical engineering applications require the evaluation of radiative configuration factors. For a number of simple geometries, closed-form expressions for configuration factors are well-cataloged[1]; however, most require some degree of numerical computation, especially if detailed surface properties are to be included in the radiative calculations. In many applications, such as combined-mode heat transfer problems, efficient and accurate numerical calculation schemes are essential. In moving boundary and time-dependent problems[2] (where exchange factors need to be calculated repeatedly), radiative calculations can be extremely computationally intensive. A comparative study of available methods for view-factor computation is found in Ref. 3.

Three methods for reducing computational error have been developed: 1) the *h*-method, involving refinement of the computational grid; 2) the *p*-method, in which the order of the approximation is increased; and 3) the *r*-method, in which nodal positions are relocated. Furthermore, these methods can be applied adaptively. The key to making adaption work effectively is in choosing robust criteria. As noted in Ref. 4, adaptive methods can increase the computational work if incorrectly applied.

Mesh refinement methods have been successfully employed in solving radiative and optical illumination problems.[3,5,7] Both adaptive *h*- and *p*-methods can be readily applied by evaluating local criteria, thus lending themselves to local adaption. The *r*-method, however, involves a global analysis. Relocating nodal positions may prove very valuable for sudden changes in the integrand, such as when blocking occurs (e.g., where a refined mesh might attempt to fit the nonshaded regions); however, redefining nodal points in more than one dimension can be algorithmically difficult.

In this note we demonstrate the advantages of adaptive *h*- and *p*-methods adaptively applied to evaluating radiative configuration factors by way of direct integration, using the finite element approach of Chung and Kim.[8] In particular, the adaptive criteria are modified as the solution of the problem proceeds in order to balance the requirements of efficiency and accuracy. Examples are drawn from simple geometries which clearly illustrate the implementation of the method for singularities associated with intersecting surfaces.

Received Aug. 23, 1991; revision received Feb. 10, 1992; accepted for publication Feb. 13, 1992. Copyright © 1991 by the American Institute of Aeronautics and Astronautics, Inc. All rights reserved.

*Assistant Professor, Department of Mechanical Engineering.
†Visiting Assistant Professor, Department of Mechanical Engineering.

View-Factor Formulation and Discretization

The general formula for the radiation configuration factor from a diffuse surface A to a diffuse surface B is expressible in terms of the angles θ_A and θ_B between the normals to the surfaces and the line connecting points r_A on surface A and r_B on surface B:

$$F_{A-B} = \frac{1}{A}\int_A \int_B \frac{\beta_{AB}\cos\theta_A \cos\theta_B}{\pi|r_A - r_B|^2}\,dA\,dB \tag{1}$$

In Eq. (1) β_{AB} is a blockage factor (zero if the line-of-sight is obstructed, and unity otherwise). While the value of the integrand in Eq. (1) is affected by the orientation of the surfaces (which decreases the integrand as sections along the surfaces become more nearly orthogonal), it is the $1/r^2$ singularity in the integrand which dominates the evaluation of the integral for connected or closely spaced surfaces.

Subdividing surfaces A and B into $(A_i)_{i=1}^{M}$ and $(B_j)_{i=1}^{N}$, the view-factor expression in Eq. (1) is discretized as

$$F_{A-B} = \frac{1}{A}\sum_{i=1}^{M}\sum_{j=1}^{N}\beta_{A_i-B_j}F_{A_i-B_j} \tag{2}$$

requiring integration for each element to element exchange:

$$F_{A_i-B_j} = \int_{A_i}\int_{B_j}\frac{\cos\theta_{A_i}\cos\theta_{B_j}}{\pi|r_{A_i} - r_{B_j}|^2}\,dB_j\,dA_i \tag{3}$$

Following Chung and Kim,[8] evaluation of Eq. (3) uses a mapping of local to global coordinates by means of the Jacobian J of the transformation, i.e.

$$dA_i = dx_{A_i}\,dy_{A_i} = |J|_{A_i}\,d\xi_{A_i}\eta_{A_i} \tag{4}$$

$$dB_j = dx_{B_j}\,dy_{B_j} = |J|_{B_j}\,d\xi_{B_j}\eta_{B_j} \tag{5}$$

As pointed out in Ref. 8, improvement in accuracy may be achieved by using higher-order finite-element interpolation functions, additional number of quadrature points, and/or more elements. The drawback to uniformly increasing quadrature order, points, or the number of elements is the computational cost.

Adaptive Criteria

Ideally, the evaluation of the integral Eq. (1) should depend on the functional form of the integrand. This is especially the case in complicated geometries where the integrand is often rapidly varying. We consider adaptive mechanisms for adequately sampling the contributions to the integral using grid refinement or local increase in the order of the quadrature based on an estimate of the local error. The objective of the adaptive scheme is to achieve a required accuracy while reducing the number of functional evaluations which grow as the product of the number of mesh points on all surfaces.

We construct the adaptive algorithm using three criteria as shown in Fig. 1. The first of these, C_1, uses the local relative error to determine whether an element should be split or its quadrature increased, and the second, C_2, evaluates the importance of the contribution of each element to the overall integral. A third criterion, C_3, is introduced to assess and modify the previous two criteria. While the rules for modification are elementary in this study, they lend themselves readily to rule-based methods in which geometries can be categorized.

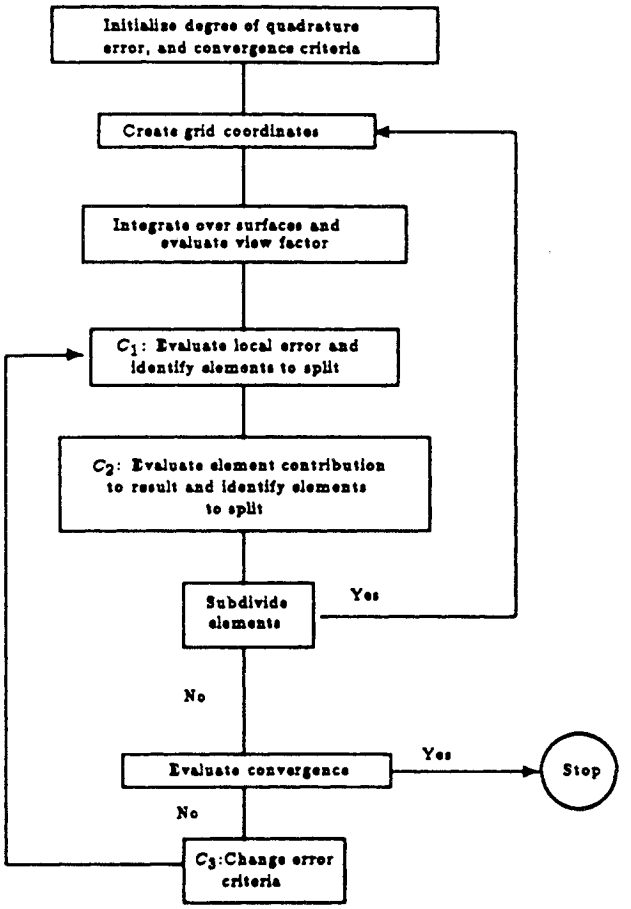

Fig. 1 Flow chart of adaptive algorithm for radiation view factors. The same logic for splitting with *h*-refinement is used for increasing the quadrature with *p*-adaption.

Criterion C_1—Modifying the Element A_i

Consider the refinement or increase in order of quadrature at step $k + 1$ by comparing the difference in the computed value of the configuration factor at iteration k and $k - 1$. Refinement is based on calculating the local error in the configuration factor between a discrete element A_i and surface B. Splitting occurs on step $k + 1$ if

$$\varepsilon_1 \leq \left| \frac{\sum_{l=1}^{L} F^{(k)}_{A_{il}-B} - F^{(k-1)}_{A_i-B}}{F^{(k)}_{A_i-B}} \right| \tag{6}$$

where A_{il}, $l = 1, 2, \ldots L$ are the elements into which A_i has been subdivided and $F^{(k)}_{A_{il}-B}$ is the configuration factor from A_i to B at iteration k. For example, subdividing each edge of a quadrilateral element gives $L = 4$. If the quadrature within each element is to be increased, the local error is similarly calculated as

$$\varepsilon_1 \leq \left| \frac{F^{(k)}_{A_i-B} - F^{(k-1)}_{A_i-B}}{F^{(k)}_{A_i-B}} \right| \tag{7}$$

where the order of quadrature p at iteration k is greater than or equal to that at iteration $k - 1$. In this study the emitting element is modified. In the event of blockage it is more usual to modify the receiving element (e.g., Refs. 5 and 6). Note that the rules for subdivision given in Eqs. (6) and (7) can include other criteria (e.g., using the local gradient of the element contributions) which is especially useful in computing exchange factors involving occluded surfaces.

Criterion C_2—Undersampling and Oversampling

Undersampling can occur whenever criterion C_1 is satisfied for a given element A_i on two successive iterations, consequently, no further modification of the element occurs. To ensure that A_i is properly sampled as the sum evolves with k, the contribution of A_i to F_{A-B} is compared to the mean contribution (less the contribution from A_i itself). Thus, if

$$\varepsilon_{2a} \leq \frac{F_{A_i-B}}{(F_{A-B} - F_{A_i-B})/(M-1)} \tag{8}$$

the element is subdivided or the order of quadrature is increased. Similarly, oversampling occurs when an element is modified too often. This occurs when the integrand is changing rapidly, yet the overall contribution to the sum is insignificant. Splitting or quadrature increase is prevented whenever element contributions to the sum are less than a prescribed tolerance ε_{2b}, i.e., if

$$\varepsilon_{2b} \geq \frac{1}{F_{A-B}} F_{A_i-B} \tag{9}$$

Criterion C_3—To Prevent the Premature Termination of the Algorithm

This occurs if there is no subdivision or increase in quadrature for any element i at iteration $k + 1$ and the convergence requirements

$$\left| \frac{F^{(k)}_{A-B} - F^{(k-1)}_{A-B}}{F^{(k)}_{A-B}} \right| \leq \alpha \tag{10}$$

are not satisfied, which typically arises from poor initial choices of ε_1 and ε_{2a}. The value α is a specified tolerance on the global relative error (i.e., the overall configuration factor from A to B), and is the stopping criterion. To force an element modification the tolerances are altered dynamically. The modification of these tolerances can be based on rules derived from an experience data base, similar in function to neural networks. (Note that choosing ε_{2b} affects the accuracy possible for a given global error α since it truncates the sum contributing to the approximation of the exchange factor integral. Acceptable levels for the truncation and global errors are set initially by the user.) To avoid ε_{2a} from becoming too small, thereby causing oversplitting, the value of ε_{2a} is reset once a split or quadrature increase has occurred at a given level k.

Numerical Results

The configuration factors are investigated for geometries involving two unit square plates lying parallel and separated by a unit distance ($\phi = 0$ deg), or intersecting at an angle ($\phi = 30$, 60, 90, 120, and 150 deg). These geometries illustrate the performance of the adaptive methods at resolving the $1/r^2$ singularity and are identical to those investigated by Chung and Kim for demonstration purposes.

Table 1 contains the analytical solutions along with the relative percentage errors achieved using various computational schemes and the CPU time in seconds (Sun SPARC 2). This absolute relative error E is defined in terms of the analytical solution F^*_{A-B}

$$E = \left| \frac{F^*_{A-B} - F_{A-B}}{F^*_{A-B}} \right| \tag{11}$$

Results for a uniform 10×10 mesh on each surface are presented, as is uniformly increasing the quadrature for each element from one to six points on this fixed 10×10 grid. These results can be scaled by noting that the computation time is proportional to the number of elements squared while the error decreases approximately as $O(h^1)$. The adaptive quadrature algorithm is implemented starting with one quadrature point per element on a 10×10 grid. The quadrature is varied from 1-, 2-, 4-, to 6-points per element using Eqs. (7–9). For the adaptive mesh, the initial grid consists of only one element per surface and subdivided elements are refined into four quadrilaterals by bisecting each side. The initial values were set at $\varepsilon_1 = 0.1$, $\varepsilon_{2a} = 4.0$, $\varepsilon_{2b} = 1.0 \times 10^{-5}$,

Table 1 Convergence of adaptive methods compared to using fixed mesh and quadrature

Analytic solution	ϕ deg 0.19983	30 deg 0.6020	60 deg 0.37120	90 deg 0.20004	120 deg 0.08700	150 deg 0.02150
Uniform grid (10 × 10) Points/element						
1	0.30% (0.92 s)	61.11% (0.98 s)	14.69% (0.98 s)	6.70% (0.97 s)	3.76% (0.97 s)	2.47% (0.99 s)
2	2.66×10^{-3} % (10.81 s)	44.23% (10.82 s)	11.18% (10.81 s)	5.03% (11.16 s)	2.66% (11.12 s)	1.65% (11.13 s)
4	2.55×10^{-3} % (162.24 s)	30.28% (162.05 s)	8.46% (163.83 s)	4.21% (163.53 s)	2.27% (162.34 s)	1.36% (166.12 s)
6	1.56×10^{-2} % (820.63 s)	22.74% (815.86 s)	6.67% (812.44 s)	3.56% (811.73 s)	1.98% (825.25 s)	1.91% (811.24 s)
Adaptive quadrature (10 × 10)						
	2.66×10^{-3} % (18.96 s) 200 pts	22.91% (83.49 s) 240 pts	6.66% (84.74 s) 240 pts	3.51% (84.06 s) 240 pts	1.98% (84.59 s) 240 pts	1.23% (103.61 s) 248 pts
Adaptive grid						
	0.29% (4.02 s) 160 pts	2.03% (337.54 s) 1876 pts	1.75% (22.70 s) 406 pts	1.97% (7.99 s) 208 pts	0.94% (15.94 s) 304 pts	2.18% (3.54 s) 100 pts

Table 2 Modification of splitting criterion based on criterion C_3 as the computation of the F^k_{A-B} for ϕ = 90-deg proceeds

k	N	ε_1	ε_{2a}
1	1	4.0	1.0
2	4	4.0	1.0
2	4	2.0	0.25
2	4	1.0	0.0625
3	10	4.0	0.0625
4	34	4.0	0.0625
5	88	4.0	0.0625
6	208	4.0	0.0625
7	412	4.0	0.0625
8	856	4.0	0.0625

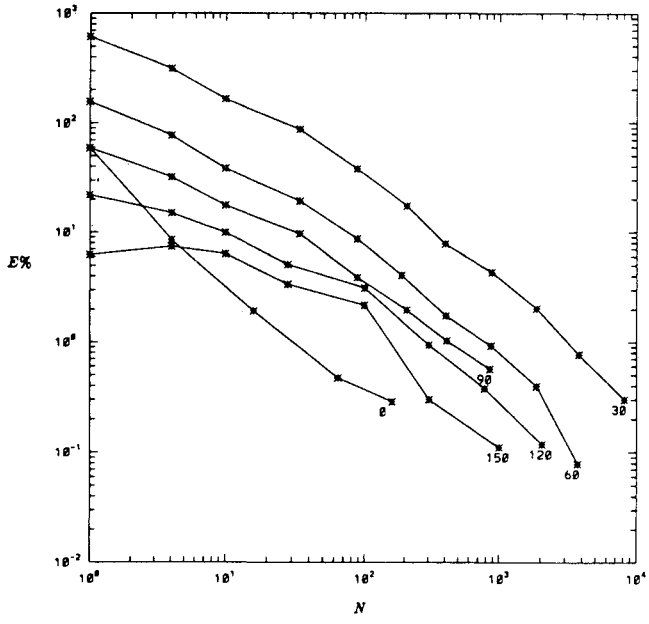

Fig. 2 Convergence histories for adaptive grid refinement with parallel plates (0 deg), and plates meeting at 30, 60, 90, 120, and 150 deg.

and $\alpha = 5.0 \times 10^{-3}$. In applying criterion C_3, ε_1 is divided by four and ε_{2a} is halved.

As expected, adaptive quadrature is more efficient at small angles of intersection than is a uniform quadrature, since only those elements close to the intersection have higher-order polynomial interpolation, whereas those far from the intersection maintain fewer quadrature points. Furthermore, consistent with the integrand being poorly represented by polynomials, the adaptive mesh with one-point quadrature in each element displays improved results over the adaptive quadrature technique. The improvement in using an adaptive mesh is most discernible when $\theta < 60$ deg. At 30 deg the adaptive mesh algorithm is estimated—using $O(h^1)$ convergence—to be about 200 times faster at reducing the error E to about 2% than the fixed-mesh approach. At large incidence angles the adaptive mesh algorithm loses its advantage. Indeed, for parallel plates it is about four times slower than the fixed mesh computation (primarily traceable to overhead and setup processing). An optimal convergence path to achieving a given accuracy over a range of geometries would use both h- and p-refinement.

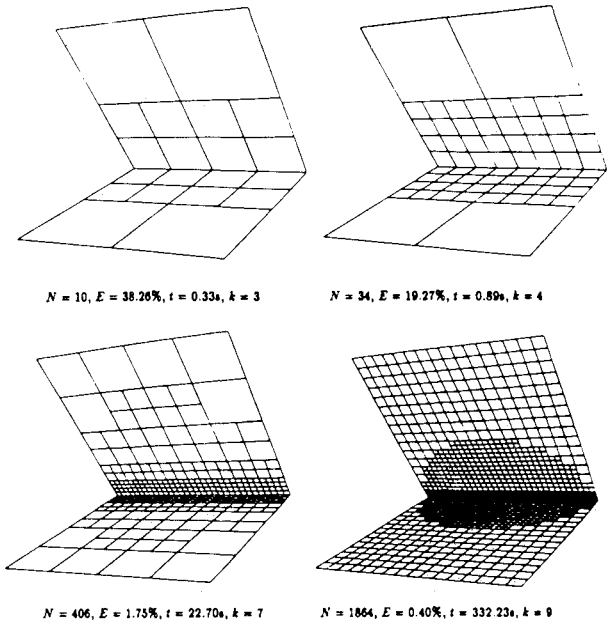

Fig. 3 Adaptive mesh refinement for two planes meeting at 60 deg showing the refined grid on both surfaces at various iteration levels k.

Figure 2 displays convergence histories using adaptive mesh refinement. The choice of ε_1 affects the initial convergence rate of the algorithm; if it is sufficiently small, uniform refinement occurs at each step. The adaption of ε_1 works very well when a sufficiently large value is chosen ($\geq 1\%$), allowing the algorithm to find a value of ε_1 and/or ε_{2a} sufficiently small to encourage splitting as needed. The initial slope of the curves

(i.e., the efficiency of the algorithm), is found to depend on this choice. The effects of adaptively modifying ε_1 and ε_{2a} are shown in Table 2. Note C_3 provides a basis for selectively testing the elements to split. Without C_3 the computation either stops before meeting the convergence criterion, or inefficiently splits every element in order to continue. Figure 3 displays a typical refinement history, showing clearly the adaptive integration of two surfaces meeting at 60 deg.

Conclusions

An effective adaptive algorithm for implementing mesh refinement or increasing quadrature in the computation of radiation configuration factors is demonstrated. While the adaptive technique functions well in simple geometries—avoiding oversplitting the domain and undersampling the integral—the results indicate the need for developing improved adaptive algorithms for finding more efficient refinement paths.

Combining h- and p-refinement is strongly recommended for complex, curved geometries, especially since h-refinement effectively captures the singularity in the integrand, while p-refinement models the trigonometric terms well.

Acknowledgment

The authors appreciate the programming assistance of Joseph P. Madden.

References

[1]Howell, J. R., *A Catalog of Radiation Configuration Factors*, McGraw-Hill, New York, 1982.

[2]Drake, D. J., "A View-Factor Method for Solving Time-Dependent Radiation Transport Problems Involving Fixed Surfaces with Intervening Participating Media," *Journal of Computational Physics*, Vol. 87, 1990, pp. 73–90.

[3]Emery, A. F., Johansson, O., Lobo, M., and Abrous, A., "A Comparative Study of Methods for Computing the Diffuse Radiation Viewfactors for Complex Structures," *Journal of Heat Transfer*, Vol. 113, May 1991, pp. 413–422.

[4]Kahaner, D., Moler, C., and Nash, S., *Numerical Methods and Software*, Prentice Hall, Englewood Cliffs, NJ, 1989, p. 155.

[5]Cohen, M. F., Greenberg, D. P., and Immel, D. S., "An Efficient Radiosity Approach for Realistic Image Synthesis," *Computer Graphics and Applications*, Vol. 6, No. 3, 1986, pp. 26–35.

[6]Campbell, A. T., and Fussell, D. S., "Adaptive Mesh Generation for Global Diffuse Illumination," *Computer Graphics*, Vol. 24, No. 4, 1990, pp. 155–164.

[7]Recker, R. J., George, D. W., and Greenberg, D. P., "Acceleration Techniques for Progressive Refinement Radiosity," *Computer Graphics*, Vol. 24, No. 2, 1990, pp. 59–66.

[8]Chung, T. J., and Kim, J. Y., "Radiation View Factors by Finite Elements," *Journal of Heat Transfer*, Vol. 104, Nov. 1982, pp. 792–795.

Combined Radiation-Convection Heat Transfer in a Pipe

J. S. Chiou*
National Cheng Kung University, Tainan, Taiwan, Republic of China

Introduction

DURING the refill and reflood periods of a postulated loss of coolant accident (LOCA), U.S. federal regulations require that for reflood rates of less than 1 in./s, clad-to-coolant heat transfer should be based on single-phase steam.

For typical reflood conditions where the fuel cladding temperature may reach 1400 K with coolant pressure in the range of 1.7–5.1 atm, the radiant heat transfer from fuel cladding to steam may become important. In a reactor safety analysis, the effect of radiation to steam is traditionally treated by the superposition model which assumes that the total Nusselt number equals the sum of the radiation and the pure convective Nusselt numbers.

The radiative and convective heat transfer are interdependent since both contain temperature-dependent material properties in such a way that a change in the heat flux due to one component causes a change in the heat flux due to the other. Therefore, the radiant energy transport should be coupled to the convection energy transports and solved simultaneously when the radiant energy becomes important. The combined radiation and convection problem is very difficult to solve due to the highly nonlinear nature of radiation transfer. In the literature, various simplifying assumptions were made depending upon the application.[1-3] Recently, Kim and Viskanta[4] studied the interaction of convection and radiation heat transfer in high pressure and temperature steam. They found that the convective Nusselt number was significantly reduced when compared with the Nusselt number of pure convection.

This study considers the effect of radiation to steam under the reflood steam cooling condition. The calculation results compared very well with the test data obtained from the steam cooling experiments performed by Larsen and Lord[5] where the pressure, power, flow rates, and the hydraulic diameter of test section were chosen to simulate the pressurized water reactor (PWR) LOCA conditions.

Analysis

The energy equations of an axisymmetric pipe flow can be written as

$$\rho C_p \left(u \frac{\partial T}{\partial x} + v \frac{\partial T}{\partial r} \right) = \frac{1}{r} \frac{\partial}{\partial r} \left[r(k + k_t) \frac{\partial T}{\partial r} \right] + u \frac{dP}{dx} + (\mu + \mu_t) \left(\frac{\partial u}{\partial r} \right)^2 - \text{div } q_R'' \quad (1)$$

where q_R'' is the radiative heat flux to the fluid element.

Before Eq. (1) can be solved, the turbulent viscosity μ_t, turbulent conductivity k_t and q_R'' must be expressed in terms of the existing variables. Van Driest's mixing length hypothesis[6] is used for μ_t, and Cebeci's model[7] is used to express the turbulent conductivity.

Landram et al.[2] proposed

$$-\text{div } q_R'' = 4K_p(T_w) \frac{T_w}{T} E_b(T_w) - 4K_p(T) E_b(T) \quad (2)$$

The Planck mean absorption coefficient K_p for steam shown in Eq. (2) is obtained from two sources. First, the exponential wide-band model developed by Edward[8] is used. Edward expressed the mean steam absorptivity by

$$\alpha_g = \frac{1}{\alpha T^4} \sum_i^m B(\nu_i, T_w) A_i \quad (3)$$

where B is the blackbody radiosity, ν is the wave number, A_i is the total absorptance of ith band, and m is the total band band number with $m = 5$ for steam. The Edward's absorption coefficient and absorptivity is referred to Beer's Law as $\alpha_g = 1 - \exp(-K_p D)$. The mean absorption coefficient can also be obtained from

$$K_p = P \left[5.6 \left(\frac{1000}{T} \right)^2 - 0.3 \left(\frac{1000}{T} \right)^4 \right] \quad (4)$$

Received Nov. 8, 1991; revision received Feb. 24, 1992; accepted for publication Feb. 25, 1992. Copyright © 1991 by the American Institute of Aeronautics and Astronautics, Inc. All rights reserved.

*Associate Professor, Department of Mechanical Engineering.